NbS_3: A unique quasi-one-dimensional conductor with three charge density wave transitions

S. G. Zybtsev,[1] V. Ya. Pokrovskii,[1,*] V. F. Nasretdinova,[1] S. V. Zaitsev-Zotov,[1] V. V. Pavlovskiy,[1] A. B. Odobesco,[1] Woei Wu Pai,[2,†] M.-W. Chu,[2] Y. G. Lin,[3] E. Zupanič,[4] H. J. P. van Midden,[4] S. Šturm,[4] E. Tchernychova,[5] A. Prodan,[4] J. C. Bennett,[6] I. R. Mukhamedshin,[7] O. V. Chernysheva,[8] A. P. Menushenkov,[8] V. B. Loginov,[8] B. A. Loginov,[9] A. N. Titov,[10] and M. Abdel-Hafiez[11,‡]

[1]*Kotel'nikov Institute of Radioengineering and Electronics of Russian Academy of Sciences (RAS), Mokhovaya 11-7, 125009 Moscow, Russia*
[2]*Center for Condensed Matter Sciences, National Taiwan University, Taipei, Taiwan, 106*
[3]*National Synchrotron Research Center, Hsinchu, Taiwan 300*
[4]*Jožef Stefan Institute, Jamova 39, SI-1000 Ljubljana, Slovenia*
[5]*Department of Materials Chemistry, National Institute of Chemistry, Hajdrihova 19, SI-1000 Ljubljana, Slovenia*
[6]*Department of Physics, Acadia University, Wolfville, Nova Scotia, Canada B0P 1X0*
[7]*Institute of Physics, Kazan Federal University, 420008 Kazan, Russia*
[8]*National Research Nuclear University Moscow Engineering Physics Institute (MEPhI), Kashirskoe sh. 31, 115409 Moscow, Russia*
[9]*National Research University of Electronic Technology (MIET), 124498, Zelenograd, Moscow, Russia*
[10]*Ural Federal University, Mira 19, 620002, Yekaterinburg, Russia*
[11]*Center for High Pressure, Science and Technology Advanced Research, 100094, Beijing, China*

(Received 30 June 2016; revised manuscript received 14 October 2016; published 4 January 2017)

We review the features of the charge density wave (CDW) conductor NbS_3 (phase II) and include several additional results from transport, compositional, and structural studies. Particularly, we highlight three central results: (1) In addition to the previously reported CDW transitions at $T_{P1} = 360$ K and $T_{P2} = 150$ K, a third CDW transition occurs at a much higher temperature $T_{P0} \approx 620 - 650$ K; evidence for the nonlinear conductivity of this CDW is presented. (2) We show that the CDW associated with the T_{P2} transition arises from S vacancies acting as donors. Such a CDW transition has not been observed before. (3) We demonstrate the exceptional coherence of the T_{P1} CDW at room temperature. The effects of uniaxial strain on the CDW transition temperature and transport are reported.

DOI: 10.1103/PhysRevB.95.035110

I. INTRODUCTION

Since Peierls transitions, at which electrons condense into charge density waves (CDWs), usually occur well below room temperature (RT), studies of CDWs in quasi-one-dimensional (1D) conductors have been usually considered a branch of low-temperature (LT) physics [1,2]. The formation of a CDW is accompanied by dielectrization (i.e., gapping) of the electronic spectrum with a corresponding drop in the electrical conductivity. The periodic lattice distortion accompanying the CDW can be studied with diffraction techniques in momentum space and scanning tunneling microscopy in real space. A notable feature of quasi-1D CDWs is their ability to slide in a sufficiently high electric field, resulting in nonlinear conductivity. This sliding is accompanied by the generation of narrowband and wideband noises. The quasi-1D CDWs also are featured with an enormous dielectric constant and metastable states originating from their deformability. In addition to these basic properties, a number of other aspects of CDW behavior has been investigated, including synchronization of CDW sliding with an external radio frequency (RF) field (the so-called Shapiro steps), coherence stimulation of CDW sliding by asynchronous RF irradiation [3], the effects of pressure [2] and uniaxial strain [4–7] on the Peierls transitions and CDW transport, and enormous electric-field-induced crystal deformations [2,8].

Several trichalcogenides of the group V metals (MX_3), namely $NbSe_3$, TaS_3 (orthorhombic and monoclinic), and phase II NbS_3 (hereafter NbS_3-II), constitute a family of typical quasi-1D CDW conductors [1,2]. Their crystal structures are formed of metallic chains surrounded by trigonal prismatic cages of chalcogen atoms. Though these compounds are apparently isoelectronic, their properties are rather diverse. For example, they display very different CDW wave vectors, indicating different degrees of filling in conduction electronic bands. A plausible reason for this variety may be the relative positioning of the chalcogen atoms [9]. Depending on their interatomic distances, chalcogen atoms can either be isolated from each other or form bonded pairs. Correspondingly, one valence electron from a chalcogen atom can either belong to the conduction band or to a localized bond.

The monoclinic polymorph NbS_3-II exhibits some fascinating features. Two CDW transitions have been reported for NbS_3-II. One CDW has a wave vector $q_1 = (0.5a^*, 0.298b^*, 0)$ [10,11] and forms at $T_{P1} =$ 330–370 K [11,12], a temperature much beyond the traditional realm of LT physics. While several basic experimental results on NbS_3-II were published in the 1980s [1,2,10,11,13–16], little subsequent work was undertaken until 2009. This gap was largely due to difficulties with synthesizing the compound: initially, NbS_3-II whiskers were only found as rare inclusions accompanying the growth of the semiconducting phase of NbS_3 (hereafter NbS_3-I) [11], which was more extensively studied [1,2,17,18]. A new phase III NbS_3 with a phase

*pok@cplire.ru
†wpai@ntu.edu.tw
‡m.mohamed@hpstar.ac.cn

 ©2017 American Physical Society

transition at 150 K was also reported [13], but was later suggested to be a subphase of NbS_3-II [8,12,19]. The synthesis conditions of NbS_3-II were established from studies in the Kotel'nikov Institute of Radioengineering and Electronics of Russian Academy of Sciences (RAS) in 2009 [8] and were successfully reproduced in the National Taiwan University. A detailed description of NbS_3-II growth conditions is presented in Ref. [8].

The most notable feature of NbS_3-II is its nonlinear transport at RT [1,2,11,12,19], associated with the CDW formed at T_{P1}. The RT CDW shows exceptionally high transport velocities and sliding coherence. The corresponding fundamental frequencies f_f, as revealed by the RF interference technique [12,19], exceed 15 GHz. The coherence of this CDW can be further improved by external asynchronous RF irradiation [3] and by uniaxial strain [20].

The Peierls transition at T_{P1} is clearly detected in transport and structural studies: a pronounced increase of resistance R, with decreasing temperature is observed near T_{P1}, while its I-V curve becomes nearly linear above 340 K. The intensities of the q_1 satellites decrease significantly above 350 K [11,21], while the satellites of the second modulation wave vector $q_0 = (0.5a^*, 0.352b^*, 0)$ remain detectable to at least 450 K.

Within NbS_3-II, low-Ohmic and high-Ohmic subphases [8,19,22] have been identified. As described previously [8], the low-Ohmic samples are prepared at 670–700 °C, and the high-Ohmic ones at 715–740 °C. Both subphases can be grown during the same run if a temperature gradient is present within the synthesis ampoule. Electron diffraction reveals a doubling of the lattice constant along the a axis (~9.65 Å) for the high-Ohmic crystals, which is absent in the low-Ohmic samples [19]. In addition to the CDW transition at T_{P1}, the low-Ohmic samples undergo a further CDW transition at $T_{P2} = 150$ K [13] as detected in the temperature-dependent resistance $R(T)$ curves [8,12,19]. Below T_{P2} nonlinear conduction with a pronounced threshold field E_t is observed. This indicates a charge transport coupled with this LT CDW. The presence of Shapiro steps definitively reveals sliding of the LT CDW [12,19]. However, RF synchronization studies reveal a surprisingly low charge density of this LT CDW. The so-called "fundamental ratio" j_c/f_f appears very low and is sample dependent [12,19] (here j_c is the CDW current density at the first Shapiro step). Attempts to find structural changes below T_{P2} using electron [10] and x-ray diffraction techniques were unsuccessful.

The LT CDW state emerges from a dielectrized state following the two CDWs formed at higher temperatures and remains a rather enigmatic charge-ordered state, which might be considered as a generalization of the usual CDW. The emergence of a new CDW in this rather resistive state is unusual, and a Keldysh-Kopaev transition [23] (the formation of an excitonic dielectric [24]) has been proposed as a possible mechanism [19].

In this paper, we present a number of new experimental results for NbS_3-II. Section II focuses on the features of the RT CDW. We report unprecedentedly high values of the CDW fundamental frequencies, as revealed by Shapiro steps. A high coherence of the RT CDW sliding is shown by the nearly complete CDW synchronization under RF power and by Bessel-type oscillations of the Shapiro steps' width vs

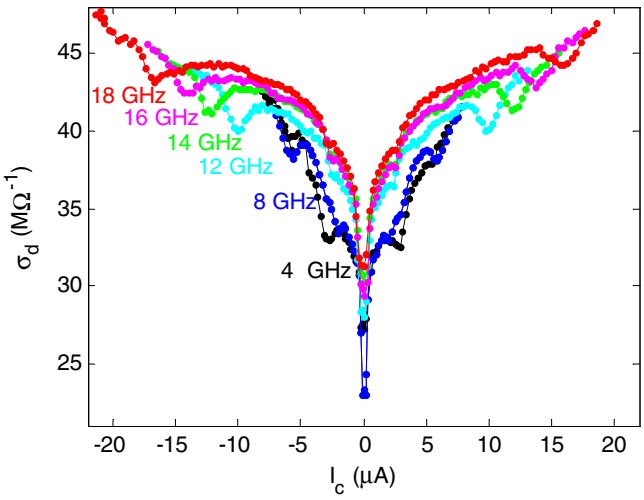

FIG. 1. The RT dependences of differential conductivity σ_d vs nonlinear current I_c under RF irradiation at different frequencies. The sample dimensions are 1.6 μm × 0.005 μm^2.

RF power. In addition, we demonstrate that the coherence can be further improved by applying strain ε parallel to the chains, i.e., along the b axis. The strain also strongly affects the CDW transition temperature T_{P1}, which decreases by approximately 80 K for $\varepsilon \approx 1.5\%$. In Sec. III, we report transport measurements at temperatures up to about 650 K. A new feature in $R(T)$ is found near 620–650 K and is attributed to the onset of an ultrahigh temperature (UHT) CDW. The evidence of nonlinear transport provided by the UHT CDW will be given. We also demonstrate that, on heating above ~800 K, the high-Ohmic subphase transforms gradually into the low-Ohmic subphase and further into a metalliclike compound. Section IV focuses on the LT CDW. Unlike the transition at T_{P1}, the LT CDW transition appears nearly insensitive to strain, as is the nonlinear conduction associated with this LT CDW. Electron-probe microanalyses (EPMA) reveal a shortage of S in the low-Ohmic samples. This suggests a coupling between the relatively high conductivity of the low-Ohmic samples and the presence of S vacancies. Though electron diffraction patterns show no changes below 150 K, the T_{P2} transition is detected by scanning transmission electron microscopy-based electron energy loss spectroscopy (STEM-EELS) and x-ray absorption near edge spectroscopy (XANES). These techniques indicate charge transfers between states coupled with S and Nb atoms, as well as with S vacancies. Nuclear magnetic resonance (NMR) studies suggest "freezing" of the condensed electronic state near T_{P2}. In Sec. V, we present an overview of the results and discuss various possible origins of the LT CDW transition. The Keldysh-Kopaev (excitonic insulator) transition [23,24] appears more consistent with the experimental data than other mechanisms of electronic condensation. In the concluding Sec. VI, we summarize the main features of the CDW states of NbS_3-II.

II. RT CDW: EFFECTS OF RF IRRADIATION AND UNIAXIAL STRAIN

The RT CDW in NbS_3-II is remarkable not only for the occurrence of sliding, but also for its extremely high sliding co-

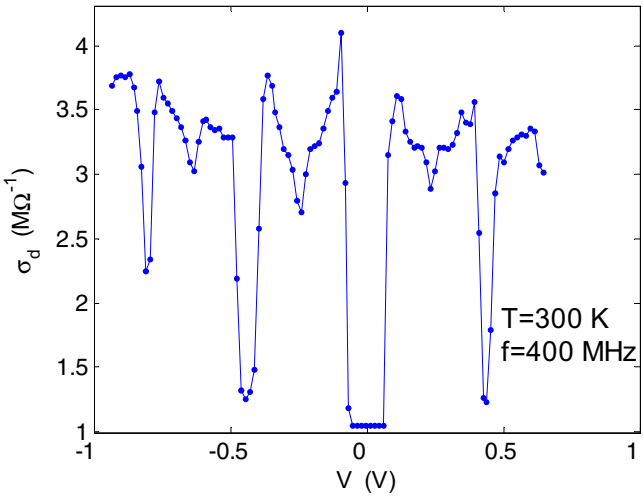

FIG. 2. An example of σ_d vs V dependence under RF irradiation at RT. The sample dimensions are 50 μm × 0.011 μm^2.

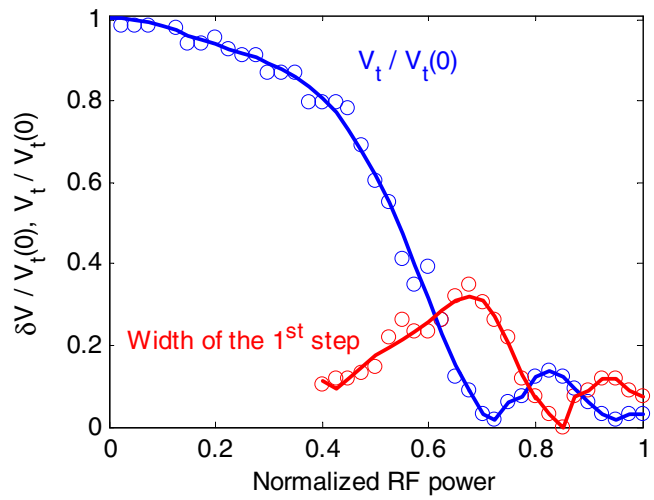

FIG. 3. A plot of a normalized Shapiro step width and V_t vs RF power (400 MHz). The sample dimensions are 50 μm × 0.011 μm^2 (see Fig. 2). The original I-V curves are in the Supplemental Material [29].

herence. The "fundamental ratio" j_c/f_f is sample independent within the experimental error (defined by the uncertainty in the sample cross-sectional area). The experimentally determined value $j_c/f_f = 18$ A/MHz/cm^2 [19] corresponds to one CDW chain per unit cell when considered within the commonly applied model of CDW sliding mode conductivity [12]. In comparison to similar compounds, this value appears unusually low; an adaptation of the conventional model may be required in the case of NbS_3-II, like for the monoclinic phase of TaS_3 [25]. Nonetheless, the universality of this "fundamental ratio" allows a precise determination of the cross-sectional area of the samples [26]. A very high coherence of the RT CDW sliding is observed in samples with nanoscale transverse dimensions. The highest fundamental frequencies are obtained in these samples. As Fig. 1 shows, Shapiro steps (the first harmonic) are observed at frequencies as high as 20 GHz. The large area per CDW chain, $s_0 = 2e/(j_c/f_f) = 180$ Å^2 [1,27], compared to other quasi-1D CDW compounds, is consistent with the relatively small amount of Joule heating of the NbS_3-II samples. They show the highest density of CDW current before burnout [19]. Based on the highest current densities ever passed through these samples, it is suggested [19] that fundamental frequencies as high as $f_f = 200$ GHz are attainable. However, synchronization of the CDW at frequencies above 20 GHz requires special arrangement of the samples for a better impedance match with RF radiation.

At a sufficiently large RF power in NbS_3-II nanodimensional samples, the RT CDW shows nearly complete synchronization: the differential conductivity σ_d of the CDW is reduced by 80–90% (Fig. 2). At the same time, the widths of the Shapiro steps show a nonmonotonic dependence on the RF power with Bessel-type oscillations. To observe such oscillations, the CDW should exhibit a high coherence. Previously, the Bessel-type oscillations were observed for $NbSe_3$ only [28]. The evolution of the I-V curves with increasing RF power is shown by a video clip in the Supplemental Material [29]. It shows the screen of a digital oscilloscope displaying the rapidly recorded I-V curves of a NbS_3-II sample. Figure 3 shows the normalized dependence of the first Shapiro step width and the threshold voltage V_t (half-width of the "zeroth step") on the RF power. A nonmonotonic suppression of V_t has been previously reported for $NbSe_3$ [30].

We recently developed techniques to apply controlled uniaxial strain to whiskerlike samples, including nanosized ones [20]. The NbS_3-II samples were stretched by bending epoxy-based substrates [20]. Studies of NbS_3-II at RT [20] and of orthorhombic TaS_3 [20,31] have demonstrated that strain can improve the CDW coherence. Figure 4 presents a set of curves showing the differential conductivity of NbS_3-II as a function of voltage V. Unlike the case of orthorhombic TaS_3 in which an ultracoherent CDW emerges through a phase transition at a critical strain [20,31], CDW coherence in the case of NbS_3-II grows gradually with ε (Fig. 4). The thresholds become sharper, the growth of σ_d above the thresholds occurs faster, and the value of the maximum CDW conductivity increases [20]. After strain removal, the threshold voltage decreases and the threshold becomes slightly sharper, while the value of resistance at $V = 0$ indicates that the sample is unstrained.

The growth of coherence with strain is also demonstrated by the effect of RF synchronization. At a fixed RF power, the Shapiro steps are more pronounced at increased strain, becoming visible directly in the I-V curves (Fig. 5).

The effect of strain appears similar to that of asynchronous RF irradiation, which also improves the coherence of the CDW sliding in a number of compounds [3,32], including NbS_3-II [3]. However, the origins of enhanced coherence in these two cases are likely different. While RF is believed to periodically draw CDW back to its starting state before it loses coherence [3], strain can change the crystal defect structure [20]. As shown in Fig. 4, the irreversible growth of coherence after strain removal may be explained by a reduction in the crystal defect density after the uniaxial deformation. For example, it is known that twin-free yttrium barium copper oxide (YBCO) crystals can be obtained by applying uniaxial pressure at 420 °C in flowing oxygen [33]. However, the major

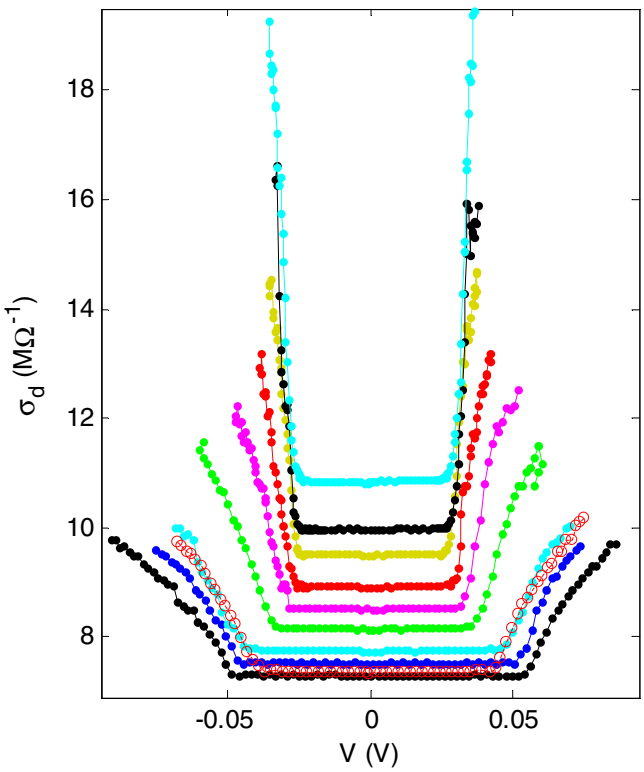

FIG. 4. The RT voltage dependencies of differential conductivity σ_d for a sample under uniaxial strain. The strain increases from $\varepsilon = 0$ (the lowest curve) to $\varepsilon \approx 1\%$ (the uppermost curve) in approximately equal steps. The curve marked with red circles was obtained after the strain was removed. The sample length L is 24 μm.

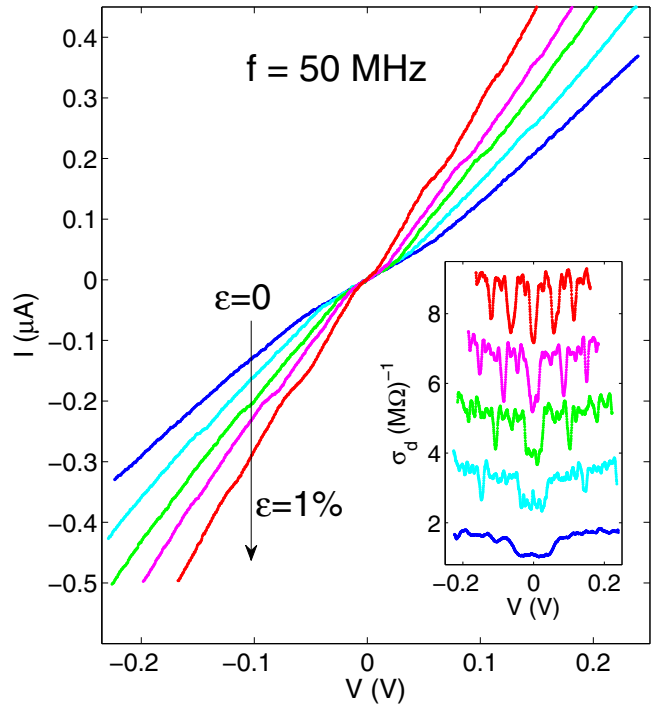

FIG. 5. RT I-V curves at different strains ε under fixed RF irradiation (50 MHz). The sample dimensions are 50 μm $\times$ 0.01 μm^2. The Shapiro steps become visible with increased ε. The inset shows σ_d vs V obtained from the I-V curves by numerical derivation. The lower curve corresponds to $\varepsilon = 0$. Other curves are shifted upward with a 1.4 MΩ^{-1} step.

part of the coherence growth is reversible (Fig. 4). This could be attributed to an alignment of the metallic chains under strain. Increased velocities of the internal acoustic modes and their reduced friction in the strained samples can also stimulate coherence of the CDW sliding through CDW-lattice coupling [8,34].

Studying strain effects of CDW transitions is important to better understand how the CDW condensate forms. Uniaxial strain decreases the anisotropy; as the interatomic distances along the conducting chains increase, the interchain distances decrease due to the Poisson contraction. The reduction in anisotropy corrugates the Fermi surfaces and decreases T_P. At the same time, 1D fluctuations are suppressed, which increases T_P. The actual changes in T_P result from the competition between these two effects. Applied uniaxial strain reduces T_P in orthorhombic TaS_3 [5,6] (but with a tendency to increase it after exceeding a critical value of ε [31]), $NbSe_3$ [5], and $K_{0.3}MoO_3$ [31]. In the monoclinic TaS_3, the lower transition is shifted downwards, while no shift was observed for the upper transition temperature for strains up to 1.5% [35].

The effects of uniaxial strain on CDW compounds have been examined less thoroughly than those of hydrostatic pressure, which is in part similar to the effect of stretching. In fact, a general feature of quasi-1D CDW compounds is also a lowering of T_P under pressure, indicating that the corrugation of Fermi surfaces has a dominant influence on T_P [2,36]. The only known exception is the monoclinic TaS_3, whose upper transition temperature increases at small pressures. It was proposed that the suppression of 1D fluctuations dominates the T_P variation in this strongly anisotropic TaS_3 polytype.

In the case of NbS_3-II, strain strongly affects the RT CDW: $\varepsilon \sim 1.5\%$ results in lowering T_{P1} from 360 K to below 280 K (Fig. 6). It is also obvious that strain sharpens the CDW transition. The decrease of T_{P1} in NbS_3-II means that, in spite of the large anisotropy [37], it is primarily dominated by Fermi-surface nesting conditions and less by the suppression of the 1D fluctuations.

The reduction of T_{P1} with ε must be taken into account in the I-V curves under strain (Fig. 4). For larger applied strains, the $\sigma_d(V)$ dependencies were measured close to T_{P1}. However, the evolution of the curves with ε cannot be attributed to the proximity of T_{P1} only. In the absence of strain, the I-V curves are smeared at temperatures close to the CDW transition [12]. Therefore, the growth of CDW coherence observed in Fig. 4, as well as the increased sharpness of the Peierls transition at T_{P1} [Fig. 6(b)], are a direct consequence of a tensile strain.

The "inverse" electromechanical effects, i.e., the impact of electrical field on the dimensions and the form of the samples, have been less studied for NbS_3-II. Similarly to orthorhombic TaS_3, $K_{0.3}MoO_3$, and $(TaSe_4)_2I$, NbS_3-II also shows electric-field-induced torsional strain. It can be observed at RT. However, the torsional angles are relatively small and are one to two orders of magnitude smaller than those observed in TaS_3. The most reliable measurement of the torsional angle as a

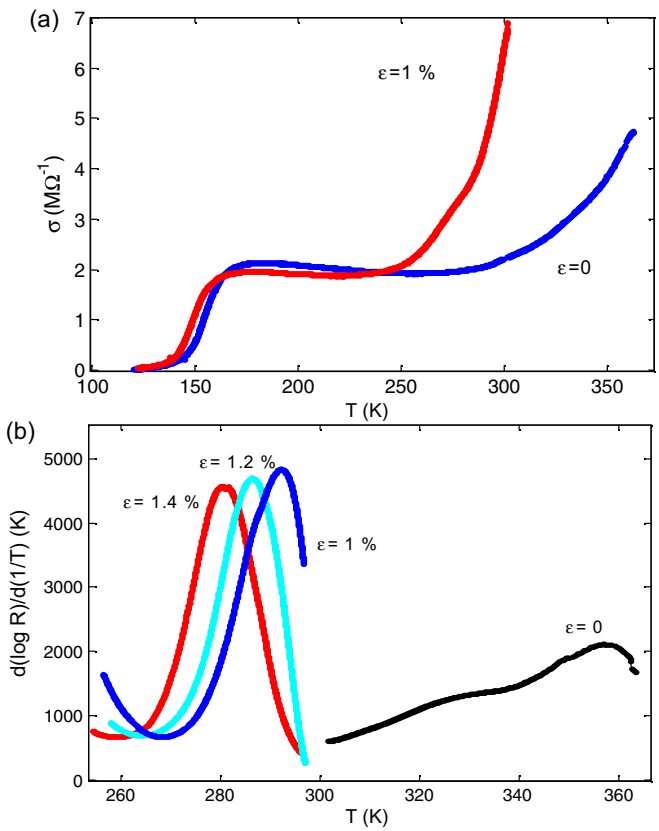

FIG. 6. (a) The initial $\sigma(T)$ curve (blue) and under ~1% of tensile strain (red). The T_{P1} transition is clearly lowered under strain. (b) The logarithmic derivatives of resistance vs T for the same sample in the vicinity of T_{P1}. The sample dimensions are 22 μm × 0.014 μm^2. Measurements under strain were not performed above 300 K due to problems with the epoxy substrates at elevated temperatures.

function of voltage is obtained with an ac voltage applied at the mechanical resonant frequency of NbS_3-II samples. Figure 7 shows two dependences of the torsional angle on current (with and without applied RF irradiation applied) measured with a

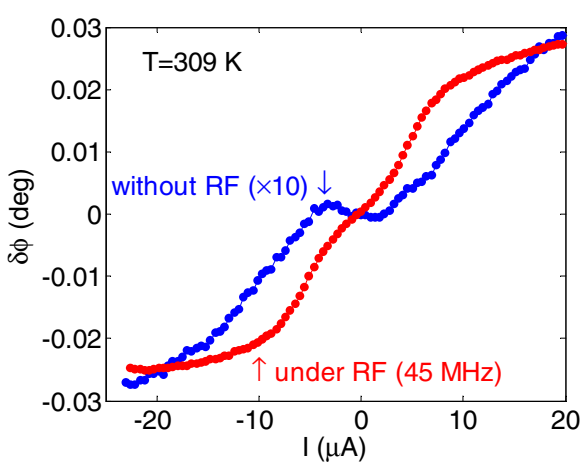

FIG. 7. Current dependence of the torsional strain amplitude. The angle is measured with the lock-in technique at a resonance frequency of 3.75 kHz. The current applied to the sample has the form of symmetric meanders. The data without RF irradiation are multiplied by 10. The sample dimensions are ~200 μm × 3.6 μm^2 [40].

lock-in technique at the lowest resonant frequency of 3.75 kHz. The applied ac voltage is symmetric, with a gradually sweeping amplitude. The torsional angle was measured optically [8]. Without RF irradiation, a threshold current for the onset of torsion was observed, like in the cases of the orthorhombic TaS_3, $K_{0.3}MoO_3$, and $(TaSe_4)_2I$ [8,38]. Radiofrequency irradiation (45 MHz) suppresses the thresholds and increases the torsional angles by an order of magnitude. This effect is in line with the coherence stimulation by an asynchronous RF irradiation [3].

The power of the RF irradiation applied at 45 MHz is sufficient to suppress the threshold down to zero, as is the case for the most of interference experiments [39] (see also Fig. 3). This is also seen in the torsional curve (Fig. 7), which has almost lost threshold features. At the same time, the torsional angles have increased by an order of magnitude. This effect seems to be in line with the coherence stimulation by an asynchronous RF irradiation [3]. In fact, coherent CDW shows larger tensile strength [31,32], i.e., larger critical strain before phase slippage. The larger CDW strain must result in a larger torsional strain of the sample.

III. THE ULTRAHIGH T_P CDW: INDICATIONS OF A PEIERLS TRANSITION AND A FRÖHLICH MODE

As mentioned in the Introduction, the diffraction patterns of NbS_3-II at 300 K show two incommensurate satellites at two CDW q vectors: $\boldsymbol{q}_0 = (0.5a^*, 0.352b^*, 0)$ and $\boldsymbol{q}_1 = (0.5a^*, 0.298b^*, 0)$ [10,11]. While the first set of satellites remain visible up to 450 K, the second set vanishes gradually above 360 K, which is close to T_{P1} [11]. When heated above 450 K under vacuum or ambient conditions, NbS_3-II crystals start to degrade.

In order to extend the measuring range and prevent crystal degradation, the $R(T)$ measurements at elevated temperatures reported herein were performed in an argon atmosphere. The temperature was monitored with a thermocouple. Heating to ~700 K and subsequent cooling was performed within several minutes. Figure 8 shows the $R(T)$ curve in a wide temperature range and very clearly reveals the transitions at T_{P1} and T_{P2}. The dependence at high temperatures, above T_{P1}, was added from a different sample during a heating cycle. Above ~600 K, a notable degradation of sample properties begins, resulting in a growth of conductivity σ. However, during fast cooling from ~700 K, the feature in the $\sigma(T)$ reappears in the same temperature range (the dynamic error in temperature determination was tens of kelvin). Therefore the $\sigma(T)$ feature around 620–650 K is attributed to a transition at T_{P0}.

As shown in Fig. 9, heating to above ~800 K gradually transforms the high-Ohmic subphase into the low-Ohmic one. Further heating transforms NbS_3-II into a compound with metallic conductivity. As discussed below, the increased conductivity may be attributed to loss of S atoms and formation of S vacancies at elevated temperature.

Figure 10 shows a series of $\sigma_d(V)$ curves for a NbS_3-II sample, recorded below and above T_{P1}. At $T > T_{P1}$, a gradual growth in conductivity at fields above 0.3 kV/cm is observed (e.g. the curve at 450 K). It is difficult to separate the effects of CDW sliding and Joule heating in these curves. However, sliding of the UHT CDW can be checked by the effect of RF

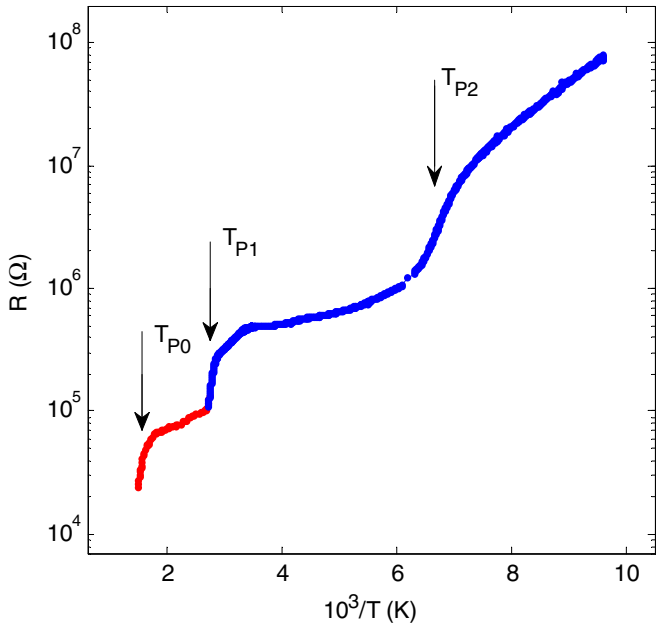

FIG. 8. A wide-range temperature dependence of NbS_3-II resistance. Data from two whiskers ($100\,\mu m \times 0.09\,\mu m^2$-high T, $126\,\mu m \times 0.06\,\mu m^2$-lower T) are combined into a single graph. The high-temperature points were obtained during a heating cycle in an Ar flow.

irradiation on the $\sigma_d(V)$ curves [3]. This effect was studied at RT, where it was possible to place the sample sufficiently close to the RF generator output for better matching. Figure 11

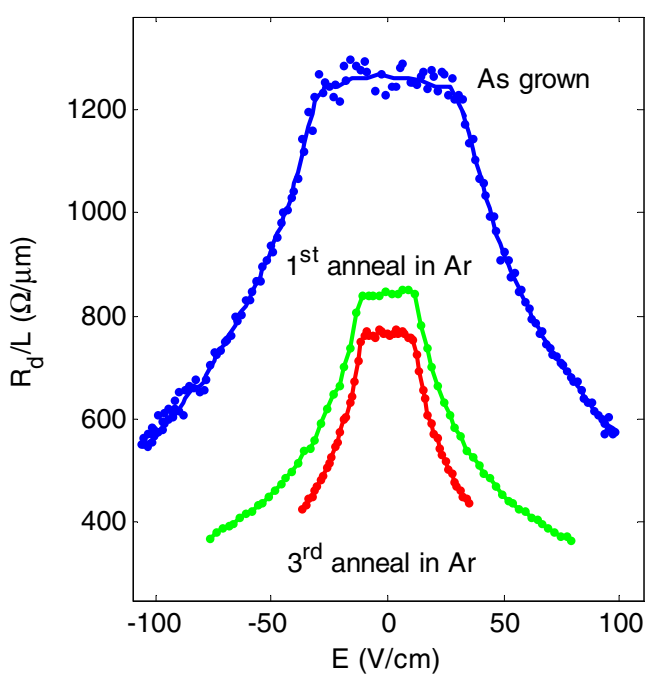

FIG. 9. Normalized RT differential resistance vs electric field of an as-grown high-Ohmic sample and after three subsequent heating/cooling cycles up to 800–850 K in an Ar atmosphere. The contact-separation $L = 1050 \rightarrow 630 \rightarrow 252\,\mu m$ (becoming shorter after each heating cycle because of new contacts).

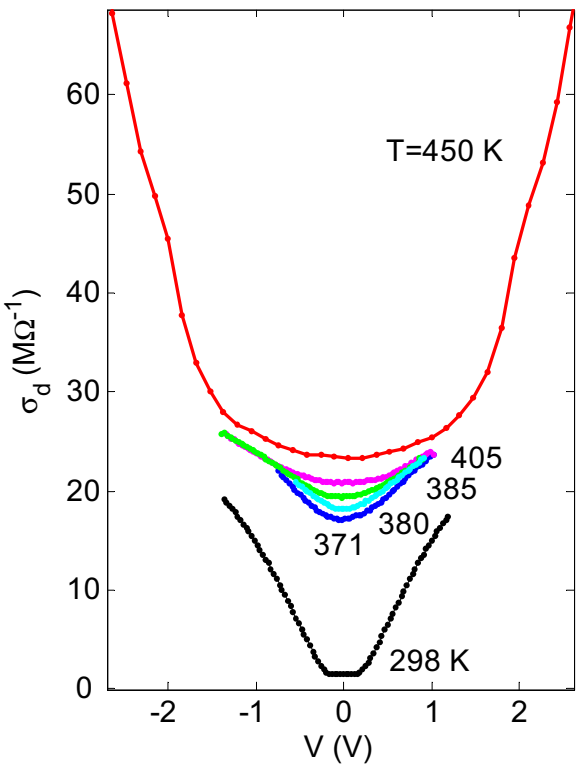

FIG. 10. The $\sigma_d(V)$ curves for a NbS_3-II sample below and above T_{P1}. The sample length is 44 μm.

shows the $\sigma_d(V)$ curves recorded at RT over a wide voltage range. At low voltages, the increase of σ_d is attributed to RT CDW sliding, which shows saturation for values above about 1 V. However, at voltages above about 5 V ($E > 10$ kV/cm),

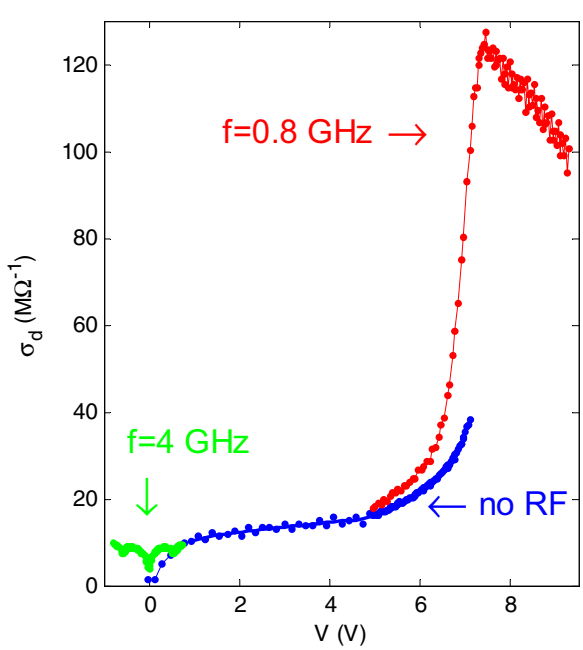

FIG. 11. RT $\sigma_d(V)$ curves with and without RF irradiation. Note the Shapiro steps under the 4 GHz irradiation. The sample dimensions are $5\,\mu m \times 5.5 \times 10^{-3}\,\mu m^2$.

σ_d grows rapidly again above the initial saturation level. To check whether this second rise comes from sliding of the UHT CDW, the effect of coherence stimulation by RF irradiation [3] was employed. One can see that, when the RF field is applied (with all other conditions kept fixed), σ_d grows faster and at lower electric fields (Fig. 11). Thus, the $\sigma_d(V)$ diagram exhibits typical features of a CDW conductor with a threshold voltage and a saturation at higher voltages. Radio frequency voltage superimposed onto a slowly sweeping dc voltage would give a trivial opposite effect, i.e., smearing out the $\sigma_d(V)$ curve (see Fig. 1 in Ref. [3]). Consequently, the observed increase of σ_d at higher voltages should be attributed to sliding of the UHT CDW. The largest current density j_c of this sliding CDW, as estimated from Fig. 11, is $\sim 5 \times 10^6$ A/cm^2; it corresponds to a fundamental frequency of $\sim$300 GHz (with $j_c/f_f = 18$ A/MHz/cm^2).

IV. THE UNUSUAL CDW FORMED BELOW 150 K

The transition at $T_{P2} = 150$ K (Fig. 8) remains the least understood. It is only observed in the low-Ohmic subphase, and the drop in specific conductivity $\Delta\sigma_s$ near 150 K is sample dependent [12,19]. These samples show a threshold in the I-V curves and Shapiro steps above the threshold voltage below T_{P2} (Figs. 12 and 13), indicating the formation of a new CDW [12,13,19]. However, the "fundamental ratio" j_c/f_f appears very low and also sample dependent. It does not exceed 6 A/MHz/cm^2 and is thus at least three times lower than the value for the RT CDW. If the charge density is assumed to be $2e$ per λ on each conducting chain, the highest values of j_c/f_f will correspond to about 1/3 of a chain per unit cell carrying the CDW. However, the lowest ratios measured below 150 K were two orders of magnitude smaller [12,19]. The difference between the RT CDW and LT CDW transport is clearly illustrated by Fig. 12, where σ_d vs nonlinear current is plotted for both CDWs under the same irradiation frequency, 400 MHz. For the first Shapiro step, the current of the LT CDW

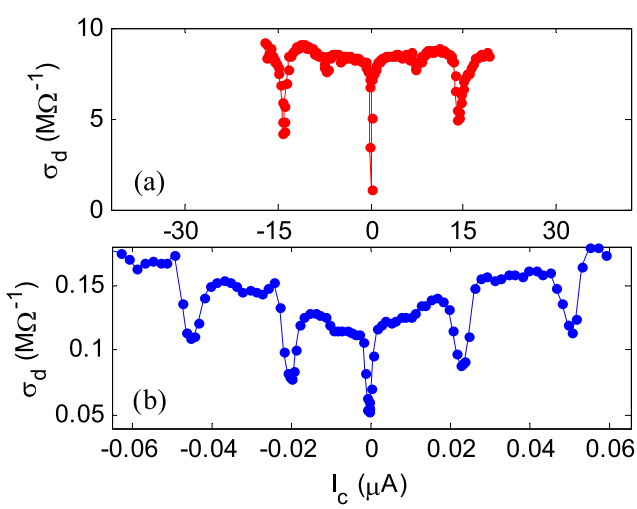

FIG. 12. σ_d vs I_c curves under 400 MHz radiation at (a) RT and (b) 122 K. The horizontal scales are adjusted to match the positions of the first Shapiro steps. The dimensions of the sample are 170 μm $\times$ 0.2 μm^2.

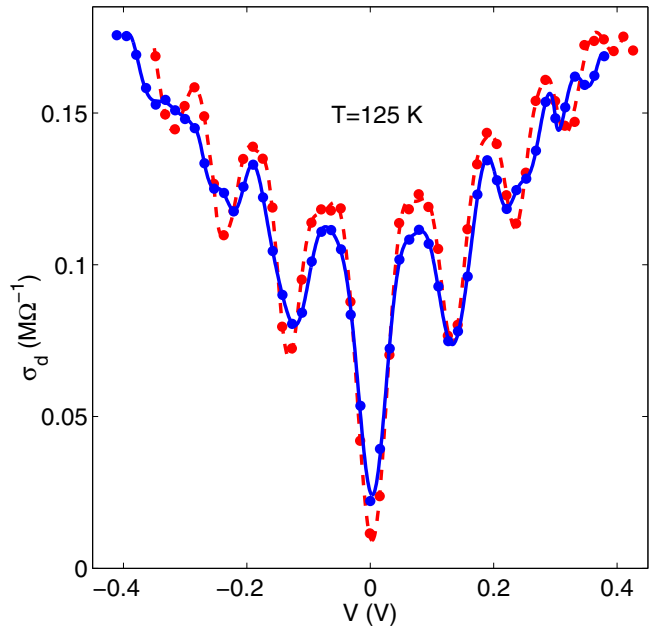

FIG. 13. σ_d vs V curves under 400 MHz radiation below 150 K. The blue (solid) line corresponds to an undeformed sample while the red (broken) curve was obtained from a stretched sample with $\varepsilon > 1\%$. The dimensions of the sample are 50 μm $\times$ 0.004 μm^2. The lines are polynomial fits of the experimental points.

is nearly three orders of magnitude lower than that of the RT CDW. The CDW current density of the LT CDW is simply too low for a classical CDW formed through a Peierls transition.

Figure 14 shows an Arrhenius plot of specific conductivities σ_s for a number of NbS_3-II samples. Shapiro steps at RT allow precise determination of their cross-sectional areas and consequently their specific conductivities. For comparison reasons, the dependence for a NbS_3-I sample [17] is added. There is a large variation between the specific conductivities of different samples. The upper group of curves corresponds to the low-Ohmic subphase and clearly reveals the 150 K transition. These samples show RT specific conductivities ranging from 10 to $3 \times 10^2 (\Omega\text{cm})^{-1}$. This range is somewhat wider than reported earlier [8,19]. Despite the large differences in the actual conductivities, which vary by over an order of magnitude, the temperature dependence $\sigma_s(T)$ for the low-Ohmic samples appears very similar on the logarithmic scale. Correspondingly, the drops in σ_s at T_{P2} appear approximately proportional to their values above T_{P2}. Thus, all the excess electrons, not gapped at T_{P0} and T_{P1}, are evidently dielectrized at T_{P2}, regardless of their actual concentration.

The conclusion is supported by the result presented in Fig. 15, where the fundamental ratio j_c/f_f of the LT CDW is shown as a function of the drop in specific conductivity $\Delta\sigma_s$ at T_{P2} [41]. The CDW current density at fixed f_f thus appears approximately proportional to $\Delta\sigma_s$.

If the single-particle conductivity above T_{P2} and the CDW conductivity below T_{P2} are provided by the same electrons, the mobility in the normal state can be estimated from the relationship between $\Delta\sigma_s$ and the "fundamental ratio" (Fig. 15). By multiplying $\Delta\sigma_s/(j_c/f_f)$ with an estimated value of $\lambda = 10$ Å, which corresponds to the wavelengths of the RT

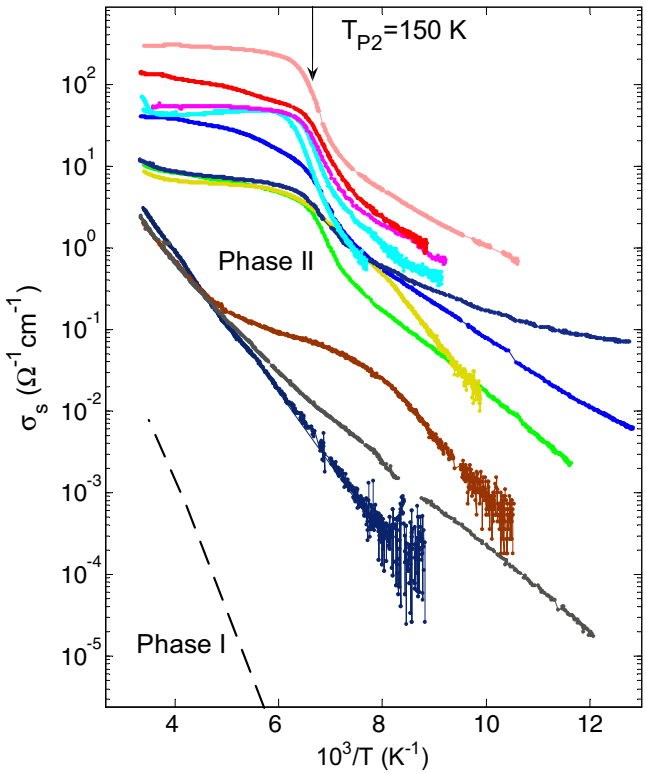

FIG. 14. A set of Arrhenius plots of σ_s for a number of NbS_3-II samples. For comparison, a typical σ_s $(1/T)$ curve for NbS_3-I is also shown [17].

and UHT CDWs, an electron mobility of about $3\,cm^2/Vs$ is obtained. For a specific conductivity $\sigma_s = 2.5 \times 10^2(\Omega cm)^{-1}$ (see Fig. 14), this mobility above T_{P2} corresponds to an electron concentration of about $5 \times 10^{20}\,cm^{-3}$, which is about 0.3 electrons per unit cell [1,2].

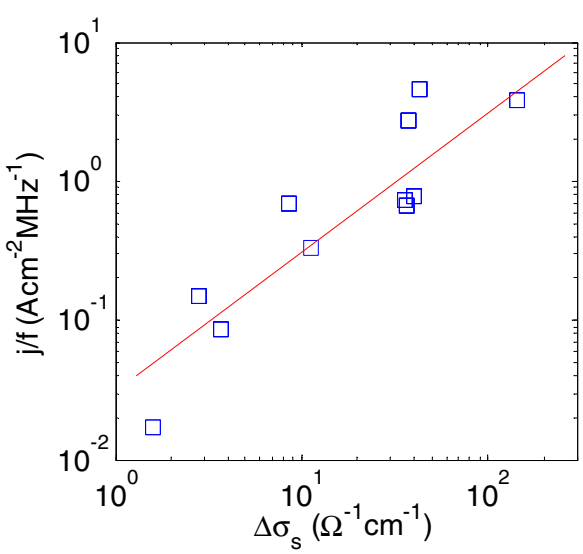

FIG. 15. The "fundamental ratio" j_c/f_f of the LT CDW vs the specific conductivity drop at T_{P2}. The straight line represents a linear approximation of the data.

Samples with $\sigma_s(300\,K) < 10(\Omega cm)^{-1}$ belong to the high-Ohmic subphase. Their pronounced dielectric behavior of the $\sigma_s(T)$ curves at RT and below (Fig. 14) indicates that the free carriers arise from thermal excitations across the Peierls gap formed at T_{P1}. A pure high-Ohmic sample shows an activation energy of about 2000 K below T_{P1}. This value is close to 2500 K, the half-value of optical gap recently reported for NbS_3-II [42]. Evidently, the number of free electrons in these samples is insufficient to condensate into a collective state. Alternatively, the transition can just become invisible in $\sigma(T)$ because of the low electron concentration.

To better understand the properties of NbS_3-II, a few further experiments were performed. The chemical composition of these samples was determined with EPMA. Reliable compositions were only obtained for samples with transverse dimensions larger than 1 μm, which all belonged to the low-Ohmic subphase. The difference in composition between the two subphases was not yet established. From a total of 15 measurements at several sample locations, we obtained a S : Nb ratio of 2.87 ± 0.04 for the low-Ohmic subphase. Independent studies, performed at National Taiwan University (NTU; Taiwan) and Moscow Institute of Physics and Technology (MIPT, Russia) gave comparable results. The nonstoichiometry indicates either the presence of S vacancies or excess Nb in the low-Ohmic samples. It has been reported previously that NbS_3 is susceptible to loss of S with heating [43]. It is therefore likely that the variation in specific conductivity found in the NbS_3-II samples is a result of S vacancies acting as donors, similar to the observed behavior of TiS_3 [44,45] and $TiSe_2$ [46,47]. Consequently, the higher concentration of S vacancies would account for the reduced electrical resistivity observed in samples, belonging to the low-Ohmic subphase. Although the EPMA measurements were not performed on the high-Ohmic samples, it is reasonable to assume that these samples are closer to the stoichiometric composition. Their transformation into the low-Ohmic phase under high-temperature treatment (Fig. 9) then can be attributed to a loss of S.

The LT CDW seems to further condense electrons from a state already dielectrized by the UHT and RT CDWs. This is rather unusual. For the conventional RT CDW, condensation of Nb d state electrons leads to a Peierls gap. To further condense electrons in the Nb d state at T_{P2}, some additional electrons can be transferred from the S p state into the Nb d state by forming $(S_2)^{2-}$ pairs. We have used XANES to probe the hole occupancy of the Nb d state and S p state by studying fluorescence-detected Nb L_3 edge (at 2375 eV) and S K edge(at 2476 eV) absorption lines. From RT to 150 K, the Nb-L_3 peak intensity decreases due to reduced hole occupancy of the Nb $4d$ state, as shown in Fig. 16(a). Similarly, the pre-edge feature (2470 eV) of the S K edge also decreases in intensity between these temperatures, as shown in Fig. 16(b). This pre-edge arises from the transition from $1s$ to a p-d mixed empty bound state when the S $3p$ state takes on a "hole" character by mixing with the Nb $4d$ states. A reduction of the S pre-edge intensity is consistent with the expectation that the Nb $4d$ hole occupancy is reduced. However, we also found that the S K edge main peak decreases in intensity by lowering the temperature from 300 to 150 K. This means that a simple scenario of electrons transferred from S $3p$ to Nb $4d$ states is questionable. Instead, some electrons are transferred to both the S $3p$ and Nb $4d$

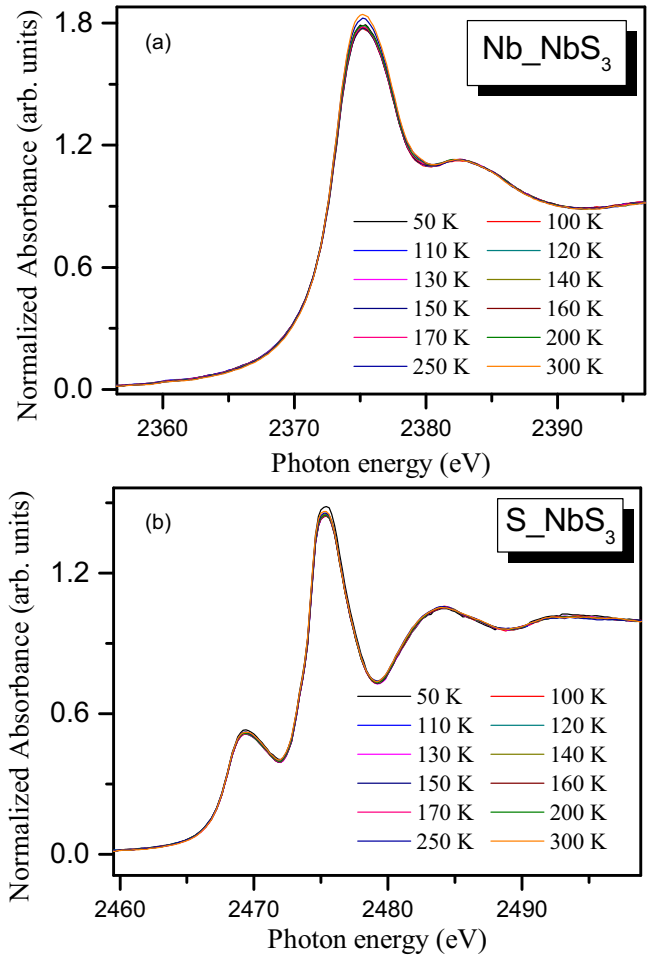

FIG. 16. Fluorescence-detected XANES. (a) Nb L_3 edge and (b) S K edge spectra between 300 and 50 K.

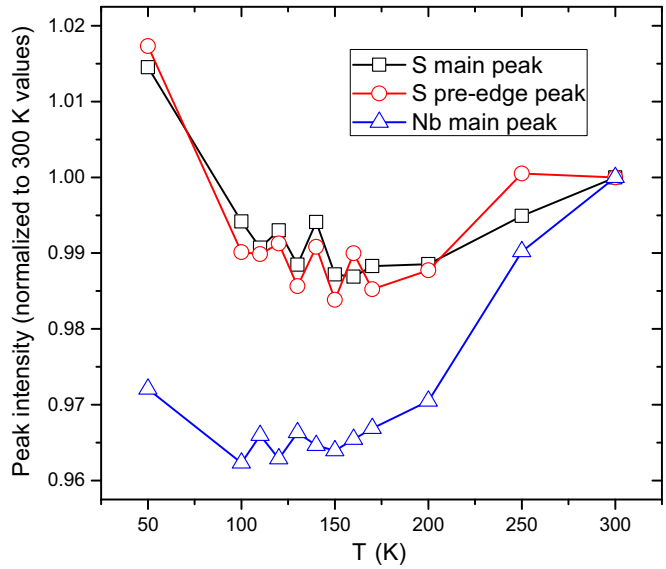

FIG. 17. The intensity ratios of the S K edge, pre-edge, and Nb L_3 edge as functions of temperature (see Fig. 16).

states. Figure 17 shows the evolutions of the Nb L_3 edge peak, the S K edge peak, and the S K edge pre-edge intensities as functions of temperature. The behavior shown in Fig. 17 is reversible with temperature.

A source of electrons to occupy Nb 4d and S 3p states could be the S vacancies acting as electron donors. The concentration of S vacancies is much larger than typical doping concentrations in semiconductor materials and therefore likely makes NbS$_3$-II a degenerate semiconductor. If the electronic structure of NbS$_3$-II is such that an electron pocket (from the Nb 4d state) and a hole pocket (from the S 3p state) coexist at the Fermi energy, a slight shift of it can either decrease or increase the hole occupancies of both the Nb 4d and S 3p states. Such an electronic structure is depicted in Fig. 1(a) of Ref. [48] and is believed to exist in WTe$_2$ [49]. As NbS$_3$-II is cooled from 300 to 150 K, thermal generation of carriers becomes less important, and the Fermi level tends to move upwards, towards the donor impurity band. This is revealed by the decrease of both the Nb L_3 edge and S K edge peak intensities observed in XANES.

By reducing the temperature from 150 to 50 K, the Nb L_3 edge and the S K edge peak intensities recover, resulting in a broad minimum at T_{P2}. While the exact cause of this phenomenon is still uncertain, the removal of electrons from Nb 4d and S 3p states could be related to exciton formation. Reduced screening is expected in low-dimensional materials and at lower temperatures, where the reduced number of free carriers leads to enhanced exciton binding energy. If the LT CDW has indeed an excitonic insulator nature, exciton formation would remove electrons below T_{P2} from the Nb 4d and S 3p states. This would also be in accord with the recovery of Nb L_3 edge and S K edge peaks below T_{P2} in XANES spectra.

We also observed a similar minimum of the Ta L_3 edge XANES in the orthorhombic phase of TaS$_3$ near $T_P = 220$ K, which is believed to be a "classical" Peierls transition [1]. However, in o-TaS$_3$ the S K edge was not simultaneously measured with the Ta L_3 edge. We therefore do not yet know whether o-TaS$_3$ and NbS$_3$-II exhibit similar XANES behaviors. This comparative measurement should be undertaken in the future.

In addition to XANES, preliminary data from STEM-EELS suggest that the local environments of S atoms change at the transition. At 105 K, the L edge of S is characterized by a single peak at 162 eV, while at 290 K, an additional peak is formed at 167 eV. Meanwhile, the M_2 and M_3 edges of Nb do not show noticeable changes. The STEM-EELS data support the suggestion that there is a change in the local environment of sulfur atoms. It is possible that changes in the S positions lead to a change in the number of S-S bonds forming $(S_2)^{2-}$ instead of $2S^{2-}$ states, or to a partial activation of S donor vacancies at low temperatures. These processes would provide another "degree of freedom" for the S atoms to change the number of free electrons without altering the Nb : S ratio.

Finally, NMR studies provide additional insight into the T_{P1} and T_{P2} transitions. The ^{93}Nb spectrum of nonoriented NbS$_3$-II powder samples in a fixed magnetic field of $B_0 = 7.5$ T clearly shows the presence of many inequivalent Nb sites in this phase. The temperature dependence of the most intense peak of the central line (the $-1/2 \leftrightarrow 1/2$ transitions) allows clear detection of the CDW transition at T_{P1}. In Fig. 18(a), the variation of the Knight shift, $K = (f/f_0 - 1) \times 100\%$, of this central

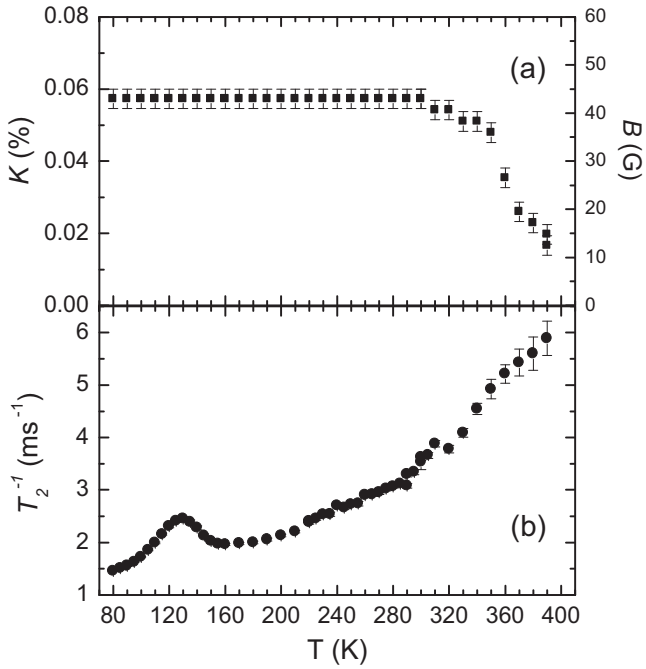

FIG. 18. (a) Temperature dependence of the Knight shift of the ^{93}Nb NMR central line. The corresponding "extra" effective magnetic field H at the ^{93}Nb nuclear sites is shown on the right scale (the external fixed field $B_0 = 7.5$ T). (b) Temperature dependence of the nuclear transverse magnetization relaxation rate T_2^{-1}.

line in the temperature range of 80–390 K is shown. Here, f is the central line peak frequency, and $f_0 = \gamma \times B_0/2\pi$ is the reference frequency, which is proportional to the external magnetic field B_0 and to the ^{93}Nb gyromagnetic ratio $\gamma/2\pi = 10.4065$ MHz/T. The Knight shift corresponds to an "extra" effective field at the nuclear site from the polarization of the conduction electrons in the presence of an external field. The right scale in Fig. 18(a) shows the estimated values of this "extra" field. Therefore, Fig. 18(a) reveals a new ordered state below T_{P1}. The most obvious reason for this is a lattice distortion coupled with CDW formation, as observed in $NbSe_3$ [50].

There is no change in the Knight shift around $T_{P2} = 150$ K [Fig. 18(a)]. However, studies of the nuclear relaxation do reveal a feature in this temperature region. The temperature dependence of the nuclear transverse magnetization relaxation rate, T_2^{-1}, measured on the same most intense peak of the central ^{93}Nb NMR line, is shown in Fig. 18(b). A maximum of $T_2^{-1}(T)$ appears at about 130 K. The loss (decoherence) of transverse nuclear magnetization happens due to different time-dependent local magnetic fields at nuclear sites. The $T_2^{-1}(T)$ dependence can be explained by the assumption that the characteristic time of such microscopic fluctuations causing relaxation is increasing as temperature decreases. At low temperatures the fluctuations slow down and their correlation time becomes comparable to the spin-echo time (tens of microseconds). In this case, decoherence of the transverse nuclear spin magnetization becomes faster and the corresponding transverse magnetization relaxation time T_2 becomes shorter. At even lower temperatures the fluctuations become very slow and their characteristic time appears much longer in comparison with the time of spin-echo formation. Consequently, the fluctuations do not contribute anymore to the transverse magnetization relaxation and T_2^{-1} begins to decrease again. Thus, the maximum in T_2^{-1} at 130 K corresponds to a "freezing" of one of the fluctuation sources causing relaxation [51,52]. The most probable candidate for such a source is an electronic or a lattice distortion, which exists at T_{P2} or even above it. Such a behavior can be expected in case of strong 1D fluctuations, where the transition signifies a 3D ordering of the CDW fluctuations (see, e.g., Ref. [53]). A similar behavior of T_2^{-1} was reported for the well-known CDW conductor $NbSe_3$ near 130 K [51], i.e. somewhat below the first CDW transition at 144 K.

Unlike the Knight shift, the relaxation of the transverse magnetization can be stimulated by fluctuation of both magnetic and electric fields. Therefore, the maximum in $T_2^{-1}(T)$ at 130 K can reveal not only a lattice but also an electronic ordering. Moreover, one can suppose that the LT CDW is mainly an electronic ordering, with corresponding lattice distortion remaining a small, secondary effect. This is consistent with the absence of changes in the Knight shift at T_{P2}, as well as the failed attempts to detect a lattice distortion at 150 K with electron diffraction [10].

Uniaxial strain can be considered a probe for the Peierls transition. Unlike T_{P1}, T_{P2} appears much less sensitive to strain [Fig. 6(a)]. Some lowering of T_{P2} is only detected at the highest applied strains. Given the same strain, the relative reduction of T_{P2} is an order of magnitude smaller than that of T_{P1}. Since the suppression of the fluctuations increases T_{P2} and the corrugation of Fermi surfaces has the opposite influence, a balance of these two effects in LT CDW might explain why T_{P2} is less sensitive to strain than T_{P1}. We note that different behaviors with respect to strain were observed in other trichalcogenides with multiple CDW transitions. In the monoclinic TaS_3, the lower transition appears to be more sensitive to strain [34] and pressure [2,35] as compared to the upper one. In $NbSe_3$, the effects of pressure and strain are different; while under pressure, the lower transition temperature decreases faster than the upper one [2,35]; the rate of decrease is much slower under uniaxial strain, especially for small strains [5]. In the case of NbS_3-II, we can suppose that either T_{P2} is more dominated by fluctuations than T_{P1}, or the transition at T_{P2} has a different origin.

The same effect of strain is observed for the nonlinear conduction of the LT CDW (Fig. 13): the I-V curves do not show notable changes up to about 1.5% strain (the apparent slight improvement of coherence was not repeated in other samples). The weak dependence of the LT CDW on strain can indicate weak coupling of this CDW with the lattice.

V. DISCUSSION

The results presented show that NbS_3-II appears to be a unique quasi-1D compound. It shows two high-temperature CDW transitions at $T_{P1} = 330-370$ K and $T_{P0} \approx 620-650$ K. Both CDWs show a Fröhlich-mode transport. The LT CDW formed below 150 K also demonstrates sliding, but its nature is not fully understood.

The LT CDW is observed only in samples belonging to the low-Ohmic subphase and is not detected in the diffraction

experiments. Both the amplitude of the feature in $\sigma(T)$ at T_{P2} and the density of the CDW current (at given f_f) depend strongly on the sample specific conductivity at RT, which can vary within the low-Ohmic subphase by more than an order of magnitude. Evidently, the variations in specific conductivity are connected with S deficiency. The excess free electrons, induced by "doping" from S vacancies, do not condense into a CDW until below 150 K. The concentration of these electrons is compatible with metals with a degenerate electronic gas. Consequently, the electronic structure can be treated in terms of new Fermi surfaces, which survived the two upper CDW transitions. The 150 K transition thus corresponds to the condensation of these free electrons and, presumably, of additional electrons released during redistribution of S bonding, into a CDW or a CDW-like formation. However, even for the low-Ohmic samples, the specific conductivity above T_{P2} is far from being metallic. The free carriers are gapped by two already existing CDWs, and the resistivity is two to three orders of magnitude above the estimated value above T_{P0} (Fig. 8). Both the T_{P2} value and the form of the feature in $\sigma(T)$ at T_{P2} (Fig. 14) show no obvious correlation with σ_s. Consequently, the transition at T_{P2} is similar for the electron concentrations varying between samples by up to 1.5 orders of magnitude. In other words, the concentration of electrons condensed into the LT CDW can vary substantially, while the characteristics of this CDW remain similar. The transition disappears or becomes invisible only if σ_s is less than $\sim 10(\Omega\text{cm})^{-1}$.

The possibility of forming a separate CDW by electrons from dopants has not been considered yet. In $NbSe_3$ and in the monoclinic phase of TaS_3, where multiple Peierls transitions are also observed, different transitions dielectrize the electrons belonging to different types of chains. In the case of NbS_3-II, some electrons originate from the S vacancies acting as donors, and they are not expected to occupy a separate band. In another case of CDW compound $K_{0.3}MoO_3$, doping with V results in extra holes, but these are gapped by the same CDW [54]. Contrary to NbS_3-II, doping in this case only results in a variation of the q vector.

No hysteresis was found in the case of NbS_3-II in the $R(T)$, $R(V)$, and $R(\varepsilon)$ measurements. Similar curves for nanosized samples did not show steps coupled with the addition/removal of a CDW wavelength ([7,55] and references therein). This could mean that the q vectors of the two upper CDWs do not vary. NbS_3-II might have features in common with $(TaSe_4)_2I$, where the CDW also shows no metastable states (see [2], pp. 357–360 and 364–367]). Probably for topological reasons [56], the CDWs cannot deform in NbS_3-II, like they do in $K_{0.3}MoO_3$, TaS_3, and a number of other compounds. If this is the case, extra free electrons cannot be incorporated into the UHT or RT CDWs. Thus, "doping" with S vacancies results in a growth of conductivity at $T > T_{P2}$, while at T_{P2}, the extra electrons become condensed into a separate CDW.

While the structure of NbS_3-I is well known [57], the structure of NbS_3-II has not been determined yet. To analyze possible lattice instabilities of known phases of NbS_3, *ab initio* density functional theory (DFT) calculations of a band structure were performed for a model structure consisting of symmetrized monoclinic unit cells of NbS_3-I. That is, we manually removed the known dimerization of NbS_3-I and placed the atoms at the mean positions of a dimerized NbS_3-I unit cell [57]. This converted the compound into a metallic state. The DFT calculations were performed in both the local density approximations by the projector augmented-wave (PAW) method [58], and in the generalized gradient approximation [59] as implemented in the ABINIT simulation package [60]. Four bands were found to cross the Fermi level in the initial filling. Two of them have relatively large flat regions corresponding approximately to ½ and ⅔ filling of the respective bands. The corrugation of Fermi surfaces appears sensitive to the electron concentration: a reduced filling of these bands flattens the Fermi surfaces and makes the compound susceptible to CDW instability. These bands may be responsible for two transitions with two q vectors. Two other bands form small near-cylindrical pockets around the Y point of the Brillouin zone and are aligned in the *Y-H* direction. They are more sensitive to doping and may eventually disappear in the case of excessive doping. Extra electrons belonging to these pockets will not be condensed into the RT or UHT CDW, but may form a new condensed CDW state.

Several possibilities for the formation of the LT CDW can be considered. The first is the Peierls transition. This would require electrons, not condensed by the CDW transitions at T_{P1} and T_{P0}, to be in nested sections of the Fermi surface. This is not a very likely scenario because of the strong dependence of the "fundamental ratio" on the electron concentration. There is a bigger probability that electrons belonging to these pockets will condense into a state in which the distance between the electrons depends on their concentration, both along and perpendicular to the chains. A candidate case is a Wigner crystal (WC), which is stabilized by the repulsive Coulomb forces. Unlike conventional CDWs, a WC is relatively weakly coupled with the lattice. This might be the reason why the LT CDW was not detected by TEM [61].

However, T_{P2}, as well as the form of the $\sigma(T)$ curve in the logarithmic scale (Fig. 14), remains stable over a wide range of electronic concentrations (nearly 1.5 orders of magnitude). Since the temperature of a Wigner crystallization depends on the concentration of electrons as a power law, the observation argues against a WC formation at 150 K.

The stability of T_{P2} might indicate that the transition at 150 K, forming a periodic potential, is not directly coupled with the electrons induced by doping. Nonetheless, these electrons, irrespective to their concentration, are accommodated into this potential and form a CDW electronic crystal. In the case of the high-Ohmic samples, this condensation remains invisible in the $\sigma(T)$ curves. The transition at T_{P2} can however show up in some other measurements, e.g., in $\sigma(T)$ studies at sufficiently high frequencies (see Fig. 4 in Ref. [15]). A kind of metal-dielectric transition was also observed close to 150 K in the NbS_3-I polytype, where the transition temperature appears stable in a wide range of pressures [18]. Thus, the 150 K transition might be an intrinsic feature of both NbS_3 polytypes and appears rather robust against pressure, strain, and doping.

Apart from the Wigner crystallization and the Peierls transition, the Keldysh-Kopaev transition [23] (known also as the formation of excitonic dielectric [24]) has been suggested as a possible mechanism for condensation of electrons in NbS_3-II at T_{P2} [19]. This transition represents a generalization of the Peierls transition, which can occur if the electron's and hole's Fermi surfaces have shapes that allow nesting. Such a

scenario is possible in a semiconductor, if the gap between the hole and electron bands is smaller than the binding energy of an exciton; in such cases, spontaneous exciton formation begins and a new electronic state develops. If the maximum and minimum of the hole and electron bands are displaced in the k-space, the vector connecting them defines the wave vector of the possible charge modulation, i.e. an excitonic CDW. Among related compounds, such an origin of CDW formation has been suggested for $TiSe_2$ [62], which is also semiconducting above the transition. Nesting of electrons and holes with formation of excitons is possible for various degrees of doping. The dielectrization is pronounced if one of the bands (the electronic one in our case) is partly filled above T_{P2}. However, if the Fermi energy is located in the gap separating the bands, like it would be in the case of a stoichiometric composition, one can expect a dielectric state already above T_{P2} with the transition remaining practically invisible in $\sigma(T)$.

Neither the possibility of sliding nor the possible values of j_c/f_f have been discussed for an excitonic CDW. One can consider a simple case of a "symmetric" excitonic CDW, which originates from the nesting of two similar electronic and hole bands, with a symmetrically positioned Fermi level ($p = n$). Such an excitonic CDW will not be charged. However, in the case of doping, its sliding can transfer charge proportional to the degree of doping.

VI. CONCLUSIONS

Our studies reveal that NbS_3-II is an interesting member of the MX_3 group. It has three CDWs: a near RT CDW at $T_{P1} = 360$ K, a LT CDW at $T_{P2} = 150$ K, and another CDW at a much higher temperature $T_{P0} \approx 620$–650 K. Each CDW presents peculiar salient features. First, the RT CDW has exceptionally high coherence and shows extremely high velocities of CDW sliding. This suggests that this RT CDW can be considered for practical applications. Second, the threshold fields and currents of the UHT CDW are impressive. Third, the LT CDW is most unusual, and a complete physical picture of its formation remains elusive. However, the available evidence suggests that a novel mechanism linked to a Keldysh-Kopaev (excitonic insulator) transition could be involved in the formation of the LT CDW state.

For readers' references, we opt to summarize the features of NbS_3-II as a list:

(1) The properties of NbS_3-II depend strongly on the growth conditions. The RT conductivity $\sigma_s(300\text{ K})$ of the samples varies from 3×10^2 to $2(\Omega\text{cm})^{-1}$.

(2) The low-Ohmic samples [$\sigma_s(300\text{ K}) = 10$–$3 \times 10^2(\Omega\text{cm})^{-1}$] are sulfur deficient with the S vacancies acting as electron donors. The gradual transformation of the high-Ohmic into the low-Ohmic ones under heating above 600 K is consistent with this conclusion.

(3) The high-Ohmic subphase [$\sigma_s(300\text{ K}) = 2$–$10(\Omega\text{cm})^{-1}$] of NbS_3-II shows two CDW transitions at $T_{P1} = 340$–370 K and at $T_{P0} \approx 620$–650 K.

(4) Apart from the transitions at T_{P0} and T_{P1}, the low-Ohmic samples show a CDW transition at $T_{P2} = 150$ K. The specific conductivity drop at T_{P2} is proportional to the specific conductivity above T_{P2}. This LT CDW is a condensate of the electrons donated by the S vacancies.

(5) All three CDWs exhibit sliding at $E > E_t$.

(6) Radiofrequency interference shows that the fundamental frequency of the RT CDW sliding can be at least 20 GHz. The extremely high coherence of this CDW is manifested in Bessel-type oscillations of E_t and of the Shapiro steps' width as a function of the RF power.

(7) At RT, the NbS_3-II samples show torsional strain. The strain grows abruptly for $E > E_t$ and can be increased by an order of magnitude with RF irradiation.

(8) Under uniaxial stretching, the RT CDW of NbS_3-II samples demonstrates many features of coherence enhancement, i.e., the threshold decreases and becomes sharper, the growth of σ_d above E_t is faster, the value of the maximum CDW conductivity increases, and the Shapiro steps under RF irradiation become more pronounced.

(9) T_{P1} is extremely sensitive to uniaxial stretching: $\varepsilon \sim 1\%$ can reduce T_{P1} to below RT. The transition at T_{P1} becomes sharper with strain, in line with the growth of the CDW coherence.

(10) Sliding of the UHT CDW can be observed below and above T_{P1}. This is proven by the effect of RF-induced coherence stimulation. The E_t value for this CDW can be on the order of 10 kV/cm at RT.

(11) The LT CDW is nearly insensitive to tensile strain. At equal strain, the relative decrease of T_{P2} is 10 times lower than that of T_{P1}. The I-V curves show no regular changes under strain up to 1%.

(12) The charge density of the LT CDW transport, i.e. the j_c/f_f value revealed by RF interference, is from 3 to 1000 times smaller than that of the RT CDW and scales with the specific conductivity above T_{P2}. The value j_c/f_f appears to be well below $2e/s_0$, which is impossible for a normal CDW.

(13) Unlike the cases of RT and UHT CDWs, no lattice distortion is observed at T_{P2} by means of diffraction techniques. The ^{93}Nb NMR study reveals a Knight shift at T_{P1}, but not at T_{P2}.

(14) A clear maximum near T_{P2} is observed in the temperature dependence of the nuclear transverse magnetization relaxation rate T_2^{-1} measured at the central ^{93}Nb NMR line. The feature in $T_2^{-1}(T)$ is interpreted by a freezing of the electronic density distortion (ordering) with cooling.

(15) Near T_{P2}, minima are observed in XANES spectra of the S K edge, K line pre-edge, and the Nb L_3 edge. The result reveals electron transfer to both S $3p$ and to Nb $4d$ states down to T_{P2}. Further cooling below T_{P2} reverses the trend of XANES intensity variation. A plausible cause for the observed XANES below T_{P2} is a formation of excitons.

(16) The condensation of the excess electrons in the low-Ohmic samples into a separate LT CDW can be explained with the rigidity of the RT and UHT CDWs, which does not allow changes of their q vectors and condensation of extra electrons. In addition, *ab initio* calculations show that these electrons may belong to additional small pockets in the Fermi surfaces and a formation of a new condensed phase.

(17) The nature of the LT CDW is not completely understood. The concept of an excitonic dielectric might explain the low sensitivity of T_{P2} to the concentration of electrons condensed into this CDW.

ACKNOWLEDGMENTS

We are grateful to A. A. Sinchenko and A. P. Orlov for the help in the strain experiments. The support of Russian Foundation for Basic Research (Grants No. 14-02-01240, No. 14-02-92015, No. 16-02-01095 and No. 17-02-01343) and the program "New materials and structures" of RAS are acknowledged. The elaboration of the "bending technique" of the uniaxial expansion was supported by the Russian Scientific Foundation (Grant No. 14-19-01644). The work of I.R.M. was supported by the Program of Competitiveness Growth of Kazan Federal University funded by the Russian Government. The support of the Ministry of Science and Technology, Taiwan (103-2923-M-002 -003 -MY3) and of the Slovenian Research Agency (ARRS) under the Slovenia-Russia bilateral project BI-RU/14-15-043 is also acknowledged. EPMA was performed, in part with the equipment of MIPT Center of Collective Usage.

[1] P. Monceau, in *Electronic Properties of Inorganic Quasi-One-Dimensional Conductors*, edited by P. Monceau (D. Reidel Publishing Company, Dordrecht, 1985), Pt. 2.

[2] P. Monceau, Adv. Phys. **61**, 325 (2012).

[3] S. G. Zybtsev and V. Ya. Pokrovskii, Phys. Rev. B **88**, 125144 (2013).

[4] J. W. Brill in *Handbook of Elastic Properties of Solids, Liquids, and Gases, Vol. 2: Elastic Properties of Solids: Theory, Elements and Compounds, Novel Materials, Alloys, and Building Materials*, edited by M. Levy (San Diego, Academic Press, 2001) Chap. 10, p. 143.

[5] R. S. Lear, M. J. Skove, E. P. Stillwell, and J. W. Brill, Phys. Rev. B **29**, 5656 (1984).

[6] V. B. Preobrazhensky, A. N. Taldenkov, and I. Yu. Kal'nova, Pis'ma Zh. Éksp. Teor. Fiz. **40**, 183 (1984) [JETP Lett. **40**, 944 (1984)].

[7] S. G. Zybtsev and V. Ya. Pokrovskii, Phys. Rev. B **94**, 115140 (2016).

[8] V. Ya. Pokrovskii, S. G. Zybtsev, M. V. Nikitin, I. G. Gorlova, V. F. Nasretdinova, and S. V. Zaitsev-Zotov, Uspekhi. Fiz. Nauk **183**, 33 (2013) [Physics-Uspekhi **56**, 29 (2013)].

[9] A. Meerschaut, J. Phys. (France) **44**, C3-1615 (1983); A. Meerschaut and J. Rouxel, in *Crystal Chemistry and Properties of Materials with Quasi-One-Dimensional Structures*, edited by J. Rouxel (D. Reidel Publishing Company, Dordrecht, 1986) p. 205–279.

[10] F. W. Boswell and A. Prodan, Physica **99B**, 361 (1980).

[11] Z. Z. Wang, P. Monceau, H. Salva, C. Roucau, L. Guemas, and A. Meerschaut, Phys. Rev. B **40**, 11589 (1989).

[12] S. G. Zybtsev, V. Ya. Pokrovskii, V. F. Nasretdinova, and S. V. Zaitsev-Zotov, Appl. Phys. Lett. **94**, 152112 (2009).

[13] A. Zettl, C. M. Jackson, A. Jánossy, G. Grüner, A. Jacobsen, and A. H. Thompson, Solid State Commun. **43**, 345 (1982).

[14] C. Roucau, J. Phys. (France) **44**, C3-1725 (1983).

[15] M. Izumi, T. Nakayama, R. Yoshizaki, K.Uchinokura, T. Iwazumi, T. Seino, and E. Matsuura, *Proceedings of International Symposium on Nonlinear Transport and Related Phenomena in Inorganic Quasi One Dimensional Conductors, Sapporo* (Hokkaido University, 1983), p. 301.

[16] B. Fisher and M. Fibich, Solid State Commun. **59**, 187 (1986).

[17] M. E. Itkis, F. Ya. Nad', S. V. Zaitsev-Zotov, and F. Lévy, Solid State Commun. **71**, 895 (1989).

[18] E. M. Dizhur, M. A. Il'ina, and S. V. Zaitsev-Zotov, Pis'ma Zh. Eksp. Teor. Fiz. **86**, 141 (2007) [JETP Lett. **86**, 132 (2007)].

[19] S. G. Zybtsev, V. Ya. Pokrovskii, S. V. Zaitsev-Zotov, and V. F. Nasretdinova, Physica B **407**, 1696 (2012).

[20] S. G. Zybtsev and V. Ya. Pokrovskii, Physica B **460**, 34 (2015).

[21] From this, one can conclude that it is the q_1 CDW that provides the nonlinear transport at RT.

[22] Evidently, in Ref. [11], the high-Ohmic samples were reported, while in Ref. [13], the low-Ohmic ones (see below).

[23] L. V. Keldysh and Yu. V. Kopaev, Fiz. Tverd. Tela **6**, 2791 (1964).

[24] W. Kohn, Phys. Rev. Lett. **19**, 439 (1967).

[25] Yu. I. Latyshev, V. E. Minakova, Ya. S. Savitskaya, and V. V. Frolov, Physica **143B**, 155 (1986).

[26] E. Slot, M. A. Holst, H. S. J. van der Zant, and S. V. Zaitsev-Zotov, Phys. Rev. Lett. **93**, 176602 (2004).

[27] Alternatively, the charge per chain transferred in time $1/f_f$ can be $1e$, as it was reported for the monoclinic phase of TaS_3 [25]. This could be the case if the CDW current in a cell is carried by two chains with opposite phases.

[28] R. E. Thorne, W. G. Lyons, J. W. Lyding, J. R. Tucker, and J. Bardeen, Phys. Rev. B **35**, 6360 (1987).

[29] See Supplemental Material at http://link.aps.org/supplemental/10.1103/PhysRevB.95.035110 for the original I-V curves and subsequent changes with increasing RF power.

[30] Yu. I. Latyshev, V. E. Minakova, and Yu. A. Rzhanov, JETP Lett. **46**, 37 (1987).

[31] S. G. Zybtsev and V. Ya. Pokrovskii, Strain-induced transformation of charge-density waves and mechanical anomalies in the quasi one-dimensional conductors TaS_3 and $K_{0.3}MoO_3$, arXiv:1602.08123.

[32] Yu. I. Latyshev and V. E. Minakova, Synth. Met., **29**, F427 (1989).

[33] R. J. Olsson, W.-K. Kwok, L. M. Paulius, A. M. Petrean, D. J. Hofman, and G. W. Crabtree, Phys. Rev. B **65**, 104520 (2002).

[34] M. V. Nikitin, S. G. Zybtsev, and V. Ya. Pokrovskii, Phys. Rev. B **86**, 045104 (2012).

[35] V. B. Preobrazhensky and A. N. Taldenkov, J. Phys. IV **3**, 57 (1993).

[36] M. Núñez-Regueiro, J.-M. Mignot, M. Jaime, D. Castello, and P. Monceau, Synth. Met. **56**, 2653 (1993).

[37] This is seen from easy cleavage of the samples, from their high aspect ratio (length/width $\sim 10^5$), from the elongated shape of the superlattice satellites [11]. The weak growth of the threshold field with cross-section reduction is also an indication of high anisotropy.

[38] V. Ya. Pokrovskii, S. G. Zybtsev, V. B. Loginov, V. N. Timofeev, D. V. Kolesov, I. V. Yaminsky, and I. G. Gorlova, Physica B **404**, 437 (2009).

[39] S. Brown and A. Zettl, *Charge Density Wave Current Oscillations and Interference Effects, in Charge Density Waves in Solids*, edited by L. P. Gor'kov and G. Grüner (Elsevier, Amsterdam: Netherlands, 1989), Vol. 25, p. 223.

[40] M. V. Nikitin, V. Ya. Pokrovskii, and S. G. Zybtsev, *Abstracts of the reports at the II International Nanoforum (works of the young scientists)*, (Russian Corporation of Nanotechnologies, Moscow, 2009), p. 174 (in Russian).

[41] Here, $\Delta\sigma_s$ corresponds approximately to the difference in σ_s between temperatures marking the half-height of the peak in the $d\log(\sigma_s)/d(1/T)$.

[42] V. Nasretdinova, V. Pokrovsky, S. Zaitsev-Zotov, and S. Zybtsev, Light-induced transition from hard to soft gap in CDW conductor NbS_3(phase II) at 77 K, Nonequilibrium Phenomena in Complex Matter: new observations and new theories, Ambrož, Krvavec, Slovenia, 13–16 December 2015, Book of Abstracts, p. 46–47, http://f7-4.ijs.si/db_images/Abstract%20book%20Krvavec%202015-final.pdf.

[43] M. Kurdi, A. Marie, and M. Danot, Solid State Commun. **64**, 395 (1987).

[44] J. O. Island, M. Barawi, R. Biele, A. Almazán, J. M. Clamagirand, J. R. Ares, C. Sánchez, H. S. J. van der Zant, J. V. Álvarez, R. D'Agosta, I. J. Ferrer, and A. Castellanos-Gomez, Adv. Mater. **27**, 2595 (2015).

[45] F. Iyikanat, H. Sahin, R. T. Senger, and F. M. Peeters, J. Phys. Chem. C **119**, 10709 (2015).

[46] M. V. Kuznetsov, I. I. Ogorodnikov, A. S. Vorokh, A. S. Rasinkin, and A. N. Titov, Surf. Sci. **606**, 1760 (2012).

[47] S. H. Huang, G. J. Shu, W. Wu Pai, H. L. Liu, and F. C. Chou (unpublished).

[48] C. Shekhar, A. K. Nayak, Y. Sun, M. Schmidt, M. Nicklas, I. Leermakers, U. Zeitler, Yu. Skourski, J. Wosnitza, Zh. Liu, Y. Chen, W. Schnelle, H. Borrmann, Yu. Grin, C. Felser, and Binghai Yan, Nat. Phys. **11**, 645 (2015).

[49] M. N. Ali, J. Xiong, S. Flynn, J. Tao, Q. D. Gibson, L. M. Schoop, T. Liang, N. Haldolaarachchige, M. Hiirschberger, N. P. Ong, and R. J. Cava, Nature **514**, 205 (2014).

[50] J. Shi, J. Chepin, and J. H. Ross, Jr., Phys. Rev. Lett. **69**, 2106 (1992).

[51] B. H. Suits and C. P. Slichter, Phys. Rev. B **29**, 41 (1984).

[52] R. R. Gainov, A. V. Dooglav, I. N. Pen'kov, I. R. Mukhamedshin, A. V. Savinkov, and N. N. Mozgova, Phys. Chem. Minerals **35**, 37 (2008).

[53] P. A. Lee, T. M. Rice, and P. W. Anderson, Phys. Rev. Lett. **31**, 462 (1973).

[54] S. Ravy, S. Rouzière, J.-P. Pouget, S. Brazovskii, J. Marcus, J.-F. Bérar, and E. Elkaim, Phys. Rev. B **74**, 174102 (2006).

[55] S. G. Zybtsev, V. Ya. Pokrovskii, and S. V. Zaitsev-Zotov, Nat. Commun. **1**, 85 (2010).

[56] In [11], it was noticed that, within the experimental accuracy, the b^* component of $q_1 + 2q_0$ equals b^*. It was suggested that q_1 could be the second harmonic of q_0. Alternatively, this relation could imply an extra condition for q_0 and q_1, forbidding their variation.

[57] J. Runsdorf and F. Jellinec, J. Sol. State Chem. **25**, 325 (1978).

[58] M. Torrent, F. Jollet, F. Bottin, G. Zerah, and X. Gonze Comput. Mat. Science **42**, 337 (2008).

[59] J. P. Perdew, K. Burke, and M. Ernzerhof, Phys. Rev. Lett. **77**, 3865 (1996).

[60] X. Gonze, B. Amadon, P. M. Anglade, J.-M. Beuken, F. Bottin, P. Boulanger, F. Bruneval, D. Caliste, R. Caracas, M. Cote, T. Deutsch, L. Genovese, Ph. Ghosez, M. Giantomassi, S. Goedecker, D. Hamann, P. Hermet, F. Jollet, G. Jomard, S. Leroux *et al.*, Comput. Phys. Commun. **180**, 2582 (2009).

[61] Another probable reason for this is the large wavelength of the LT CDW. To estimate the $\boldsymbol{q}_2$ vector, we must first establish the electronic structure of NbS_3. The two IC components of the two upper $\boldsymbol{q}$-vectors are close to $1/3b^*$. If we assume that at T_{P0} two chains per unit cell are gapped, and at T_{P1}, one (as found by the RF interference [19,12]), the relation $(q_{1b} + 2q_{0b})/3 = 1/3b^*$ gives the value of the "average" $\boldsymbol{q}$ vector and can be interpreted as an indication of 1/3 filling of the electronic band. Then the detailed formula of NbS_3 can be written as $2Nb^{5+}Nb^{4+}2(S_2)^{2-}5S^{2-}$. In this case, there are 2/3 free electrons per Nb atom. Sulfur accepts either one or two electrons per atom. Then 5% S vacancies can provide 0.15 to 0.3 electrons per Nb atom, and the correspondent CDW wavelength can range from 6.7 to 13.3 periods along the b axis. It is a good challenge to find such a distortion.

[62] F. J. Di Salvo, D. E. Moncton, and J. V. Waszczak, Phys. Rev. B **14**, 4321 (1976).